PROC. OF JSCE,
No. 232, DEC. 1974

AN APPROXIMATE METHOD FOR ANALYSING EARTHQUAKE MOTIONS OF AN INHOMOGENEOUS ELASTIC LAYER

*By Masayuki HORI**

1. INTRODUCTION

It is known that damage to engineering structures during earthquakes depends upon the nature of the arriving seismic waves as well as on the properties of the structures. The characteristics which are of major interest to engineers for the purpose of design are the intensity, the frequency composition and the total duration of the earthquake motion. Generally, such features are functions of the following three factors:

(1) the source mechanism,
(2) the material properties of the earth media along the various paths through which the seismic waves travel, and
(3) the local geological conditions of the site under consideration.

The complicated nature of the earthquake source mechanism, the irregular structure of the earth's mantle and crust, and the difficulty of taking significant measurements make it difficult to elucidate the real influences on the ground motion. For the purpose of designing earthquake resistant buildings and analysing ground shaking, however, (2) and (3) of above three factors are especially significant in earthquake engineering. A great deal of effort has gone into how to take into account the material properties and the local geological conditions into the response analyses such as the wave propagation method[1)~6)] and the lumped mass method.[7),8)]

In general, the ground formation near the surface is very complicated and the dynamic properties of earth materials vary with the confining pressure as investigated by Hardin and Richart.[9)] Moreover, it is often that throughout whole layered formation, the S-wave velocity and the density of a layer are greater as depth increases. In other words, it is possible to represent the vertical distribution of dynamic moduli and densities with some suitable continuous function of which value increases monotonously with depth. In this paper, we will call this layered system an inhomogeneous layer. Some investigators[10)~12)] have dealt with the problem of the response characteristics of the inhomogeneous elastic soil layer due to SH-wave, which is incident vertically to it, and obtained the general solution under any inhomogeneous condition by solving the partial differential equation mathematically. But they did not discuss the calculating method used in order to obtain the underground motion from the surface record.

In this paper, an approximate technique will be presented to analyse the response of an inhomogeneous elastic superficial soil layer subjected to an incident earthquake motion at the base rock and to calculate the underground motions from observed earthquake records at the surface for the purpose of engineering applications. This is based on the multiple reflection theory of wave. The accuracy of this technique is examined by a comparison with the exact solutions.

2. BASIC EQUATIONS FOR THE MULTIPLE REFLECTION THEORY FOR THE MULTI-LAYERED SYSTEM

Here we consider the ground consisting of horizontal multi-layers overlying an elastic half-space as shown in Fig. 1. H_i and ρ_i are the thickness and the density, and U_i and D_i are the ascending wave and the descending wave in ith layer, respectively. A set of n coordinates, z_i, $i=1, 2, \cdots, n$, is defined as shown in Fig. 1. A relationship between shear wave velocity c_i and traveling time τ_i is

* Dr. Eng., Post Doctoral Fellow, The University of Western Ontario, Canada.

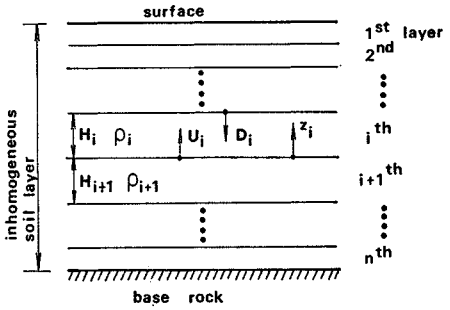

Fig. 1 Inhomogeneous Layer Divided into n Layers.

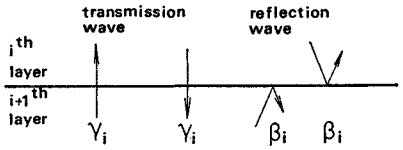

Fig. 2 Definition of Transmission and Reflection Coefficients.

$$\tau_i=\frac{H_i}{c_i}. \quad \cdots\cdots(1)$$

The transmission and reflection coefficients of a wave at the boundary between the ith and $(i+1)$th layers are defined as shown in Fig. 2. The impedance ratio α_i is given by

$$\alpha_i=\frac{\rho_i c_i}{\rho_{i+1}c_{i+1}}. \quad \cdots\cdots(2)$$

Each coefficient shown in Fig. 2 is expressed in term of α_i as follows;

$$\left.\begin{aligned}\gamma_i&=\frac{2}{1+\alpha_i}, \quad \gamma_i'=\frac{2\alpha_i}{1+\alpha_i}\\ \beta_i&=\frac{1-\alpha_i}{1+\alpha_i}, \quad \beta_i'=\frac{\alpha_i-1}{1+\alpha_i}.\end{aligned}\right\} \quad \cdots\cdots(3)$$

The equation of a shear wave which propagates vertically only, is indicated as

$$\frac{\partial^2 u_i(t,z_i)}{\partial t^2}=\frac{G_i}{\rho_i}\frac{\partial^2 u_i(t,z_i)}{\partial z_i^2}. \quad \cdots\cdots(4)$$

Its solution is denoted by the sum of the ascending and the descending waves

$$u_i(t,z_i)=U_i\left(t-\frac{z_i}{c_i}\right)+D_i\left(t-\tau_i+\frac{z_i}{c_i}\right) \quad \cdots\cdots(5)$$

where, $u_i(t,z_i)$ is the horizontal displacement at the time t and the coordinate z_i in the ith layer and G_i is the shear modulus. The displacements at the boundaries, $z_i=H_i$ and $z_i=0$ as shown in Fig. 3, are given by

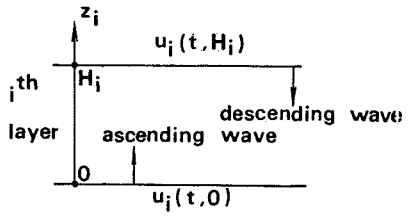

Fig. 3 The ith Layer.

$$\left.\begin{aligned}u_i(t,H_i)&=U_i(t-\tau_i)+D_i(t)\\ u_i(t,0)&=U_i(t)+D_i(t-\tau_i).\end{aligned}\right\} \quad \cdots\cdots(6)$$

If the wave record observed at the ground surface is given by $u_s(t)$, the relation between the ascending and the descending waves, because of free shear stress, is as follows;

$$U_1(t-\tau_1)=D_1(t)=\frac{1}{2}u_s(t). \quad \cdots\cdots(7)$$

In general, the following relationships between the ascending and the descending waves appear;[13]

$$U_i(t)=\gamma_i U_{i+1}(t-\tau_{i+1})+\beta_i' D_i(t-\tau_i) \quad \cdots\cdots(8)$$

$$D_i(t)=\beta_{i-1}U_i(t-\tau_i)+\gamma_{i-1}'D_{i-1}(t-\tau_{i-1}). \quad \cdots\cdots(9)$$

The relationship between the incident wave $u_0(t)$ and the ascending and the descending waves in the nth layer is given by

$$u_0(t)=\frac{1}{\gamma_n}\{U_n(t)+\beta_n' D_n(t-\tau_n)\}. \quad \cdots\cdots(10)$$

If either $u_s(t)$ or $u_0(t)$ is known, the transient motion in all layers during an earthquake can be calculated successively in the time region, by solving the simultaneous equations of Eqs. (7), (8), (9) and (10).

3. CALCULATION OF UNDERGROUND MOTION FROM THE SURFACE RECORD[14]

3.1 Derivation of Approximate Equations

We will postulate that the elastic inhomogeneous surface layer lies upon the base rock and the incident earthquake motion propagates vertically upward from the base rock to the surface layer as an SH-wave.

The elastic inhomogeneous layer is regarded as a kind of multi-layered system consisting of an infinite number of homogeneous elastic layers with infinitesimally small thickness, of which rigidity and density change successively in regular order. Therefore, at first the inhomogeneous layer with a thickness of H is divided into n homogeneous layers. The recurrent equation

to express the motion in an arbitrary layer, in terms of known surface motion $u_s(t)$, is derived by means of the multiple reflection theory. By letting the number of the divided layers approach infinity, the recurrent equation can be transformed into the integral form. At the stage of obtaining the recurrent equation, the terms of the combinations of the transmission coefficients γ_i, γ_i', $i=1, 2, \cdots, i$ and the reflection coefficients β_i, β_i', $i=1, 2, \cdots, i$, will appear in the equation. Since the characteristic impedance increases with depth as assumed before, an impedance ratio α_i is in the range of

$$0<\alpha_i<1 . \quad \cdots\cdots(11)$$

At the limit where n goes to infinity, α_i approaches unity. Therefore, it is found from Eq. (3) that γ_i and γ_i' approach unity, β_i and β_i' both approach zero. In deriving the approximate equations as described below, only the terms of the first and second order of the reflection coefficients β_i and β_i', $i=1, 2, \cdots, i$, are considered and the terms of the higher order are neglected, because they are infinitesimally small quantities.

From Eq. (7)

$$U_1(t)=\frac{1}{2}u_s(t+\tau_1), \qquad D_1(t)=\frac{1}{2}u_s(t) . \quad \cdots\cdots(12)$$

The ascending wave in the 2nd layer can be expressed by the following equation from Eqs. (8) and (12);

$$U_2(t)=\frac{1}{2\gamma_1}\{u_s(t+\tau_1+\tau_2)-\beta_1' u_s(t-\tau_1+\tau_2)\} . \quad \cdots\cdots(13)$$

Upon repeated application of the above recurrent equation,

$$\begin{aligned}U_3(t)=\frac{1}{2}\Big\{&\frac{1}{\gamma_1\gamma_2}u_s(t+\tau_1+\tau_2+\tau_3)\\&-\frac{\beta_1'}{\gamma_1\gamma_2}u_s(t-\tau_1+\tau_2+\tau_3)\\&-\frac{\beta_2'\gamma_1'}{\gamma_2}u_s(t-\tau_1-\tau_2+\tau_3)\\&-\frac{\beta_1\beta_2'}{\gamma_1\gamma_2}u_s(t+\tau_1-\tau_2+\tau_3)\Big\} ,\end{aligned}$$

$$\begin{aligned}U_4(t)=\frac{1}{2}\Big\{&\frac{1}{\gamma_1\gamma_2\gamma_3}u_s(t+\tau_1+\tau_2+\tau_3+\tau_4)\\&-\frac{\beta_1'}{\gamma_1\gamma_2\gamma_3}u_s(t-\tau_1+\tau_2+\tau_3+\tau_4)\\&-\frac{\gamma_1'\beta_2'}{\gamma_2\gamma_3}u_s(t-\tau_1-\tau_2+\tau_3+\tau_4)\\&-\frac{\gamma_1'\gamma_2'\beta_3'}{\gamma_3}u_s(t-\tau_1-\tau_2-\tau_3+\tau_4)\\&-\frac{\beta_1\beta_2'}{\gamma_1\gamma_2\gamma_3}u_s(t+\tau_1-\tau_2+\tau_3+\tau_4)\\&-\frac{\beta_2\beta_3'}{\gamma_1\gamma_2\gamma_3}u_s(t+\tau_1+\tau_2-\tau_3+\tau_4)\\&-\frac{\gamma_2'\beta_1\beta_3'}{\gamma_1\gamma_3}u_s(t+\tau_1-\tau_2-\tau_3+\tau_4)\Big\} ,\end{aligned}$$

$\cdots\cdots\cdots\cdots\cdots\cdots\cdots\cdots$

we finally arrive at Eq. (15) in an arbitrary ith layer by taking into account Eq. (14),

$$\beta_i=\beta_i', \qquad i=1, 2, \cdots, i \quad \cdots\cdots(14)$$

$$\begin{aligned}U_i(t)=\frac{1}{2}\Big\{&\Big(\prod_{k=1}^{i-1}\frac{1}{\gamma_k}\Big)u_s\Big(t+\sum_{k=1}^{i}\tau_k\Big)+\sum_{k=1}^{i-1}\beta_k\Big(\prod_{j=k}^{i-1}\frac{1}{\gamma_j}\Big)\Big(\prod_{l=1}^{k-1}\gamma_l'\Big)u_s\Big(t+\sum_{k=1}^{i}\tau_k-\sum_{m=1}^{k}\tau_m\Big)\\&+\sum_{\substack{p=1\\(p<q)}}^{i-1}\sum_{q=1}^{i-1}\beta_p\beta_q\Big(\prod_{r=1}^{p}\frac{1}{\gamma_r}\Big)\Big(\prod_{s=p+1}^{q-1}\gamma_s'\Big)\Big(\prod_{t=q}^{i-1}\frac{1}{\gamma_t}\Big)u_s\Big(t+\sum_{k=1}^{i}\tau_k-2\sum_{m=p+1}^{q}\tau_m\Big)\Big\} . \quad \cdots\cdots(15)\end{aligned}$$

Similarly, for the descending wave in the ith layer

$$\begin{aligned}D_i(t)=\frac{1}{2}\Big\{&\Big(\prod_{k=1}^{i-1}\gamma_k'\Big)u_s\Big(t-\sum_{k=1}^{i}\tau_k\Big)+\sum_{k=1}^{i-1}\beta_k\Big(\prod_{j=1}^{k}\frac{1}{\gamma_j}\Big)\Big(\prod_{l=k+1}^{i-1}\gamma_l'\Big)u_s\Big(t-\sum_{k=1}^{i}\tau_k+2\sum_{m=1}^{k}\tau_m\Big)\\&+\sum_{\substack{p=1\\(p<q)}}^{i-1}\sum_{q=1}^{i-1}\beta_p\beta_q\Big(\prod_{r=p}^{q}\frac{1}{\gamma_r}\Big)\Big(\prod_{s=1}^{p-1}\gamma_s'\Big)\Big(\prod_{t=q+1}^{i-1}\gamma_t'\Big)u_s\Big(t-\sum_{k=1}^{i}\tau_k+2\sum_{m=p+1}^{q}\tau_m\Big)\Big\} . \quad \cdots\cdots(16)\end{aligned}$$

At the limit that the number of the divided layers goes to infinity, that is to say, thickness of each layer is infinitesimally small, Eqs. (15) and (16) can be expressed by the integral forms:

$$\begin{aligned}U(t,x)=\lim_{\substack{i\to\infty\\ \tau_1,\tau_2,\cdots,\tau_i\to 0}}U_i(t)=\frac{1}{2}A(x)\Big\{&u_s\Big(t+\int_0^x\frac{dx}{c(x)}\Big)+\int_0^x B(y)u_s\Big(t+\int_0^x\frac{dx}{c(x)}-2\int_0^y\frac{dy}{c(y)}\Big)\\&+\int_0^x B(z)\int_0^z B(w)u_s\Big(t+\int_0^x\frac{dx}{c(x)}-2\int_w^z\frac{dw}{c(w)}\Big)dw\,dz\Big\} , \quad \cdots\cdots(17)\end{aligned}$$

$$\begin{aligned}D(t,x)=\lim_{\substack{i\to\infty\\ \tau_1,\tau_2,\cdots,\tau_i\to 0}}D_i(t)=\frac{1}{2}A(x)\Big\{&u_s\Big(t-\int_0^x\frac{dx}{c(x)}\Big)+\int_0^x B(y)u_s\Big(t-\int_0^x\frac{dx}{c(x)}+2\int_0^y\frac{dy}{c(y)}\Big)\\&+\int_0^x B(z)\int_0^z B(w)u_s\Big(t-\int_0^x\frac{dx}{c(x)}+2\int_w^z\frac{dw}{c(w)}\Big)dw\,dz\Big\} . \quad \cdots\cdots(18)\end{aligned}$$

In the above equations, the new coordinate system is used as shown in Fig. 4. The first term is for the direct transmission wave, and the second and third are for the wave which is reflected once in the case of the second term and twice in the case of the third in the inhomogeneous layer. The physical meaning of each term is shown in Fig. 5. $A(x)$ and $B(x)$ are functions of depth and they correspond to the transmission and the reflection coefficients which are discussed in **3.2.** $c(x)$ is the distribution function of shear wave velocity. From Eq. (5) the displacement $u(t, x)$ at the arbitrary depth is given by

$$u(t, x)=U(t, x)+D(t, x)\,. \quad \cdots\cdots\cdots\cdots(19)$$

Also, the incident motion $u_0(t)$ is obtained from

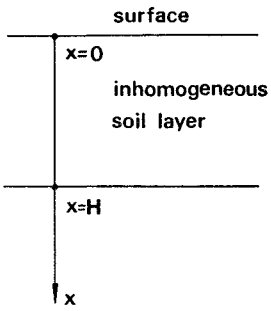

Fig. 4 Coordinate System for the Inhomogeneous Layer.

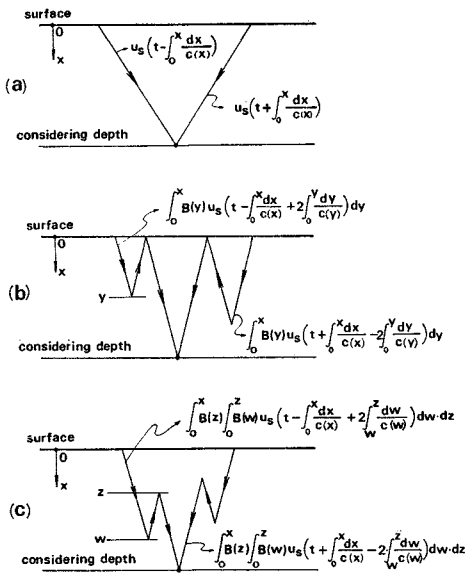

Fig. 5 (a) Direct Transmission Wave, (b) the First Order Reflection Wave and (c) the Second Order Reflection Wave.

$$u_0(t)=\frac{1}{\gamma_n}\{U(t, H)+\beta_n D(t, H)\} \quad \cdots\cdots\cdots(20)$$

where, γ_n and β_n are the transmission and the reflection coefficients at the interface between the superficial layer and the base rock.

3.2 Discussion about $A(x)$ and $B(x)$

$A(x)$ is the limit value of the product of the transmission coefficients and is expressed by

$$A(x)=\lim_{i\to\infty}\prod_{k=1}^{i-1}\frac{1}{\gamma_k}=\lim_{i\to\infty}\prod_{k=1}^{i-1}\gamma'_k\,. \quad \cdots\cdots\cdots(21)$$

From Eq. (3)

$$\frac{\gamma'_k}{\gamma_k}=\alpha_k \quad \cdots\cdots\cdots\cdots\cdots\cdots\cdots\cdots\cdots\cdots(22)$$

so that

$$\frac{\prod_{k=1}^{i-1}\gamma'_k}{\prod_{k=1}^{i-1}\gamma_k}=\prod_{k=1}^{i-1}\alpha_k=\frac{\rho_1 c_1}{\rho_2 c_2}\cdot\frac{\rho_2 c_2}{\rho_3 c_3}\cdot\ \cdots\ \cdot\frac{\rho_{i-2}c_{i-2}}{\rho_{i-1}c_{i-1}}$$

$$=\frac{\rho_1 c_1}{\rho_{i-1}c_{i-1}}\,. \quad \cdots\cdots\cdots\cdots(23)$$

If the distribution function of the characteristic impedance is given by $\chi(x)=\rho(x)c(x)$, we obtain the following equation from Eq. (23);

$$\lim_{i\to\infty}\prod_{k=1}^{i-1}\alpha_k=\frac{\chi(0)}{\chi(x)}\,. \quad \cdots\cdots\cdots\cdots\cdots\cdots(24)$$

Consequently, $A(x)$ can be expressed by $\chi(x)$ from Eqs. (21) and (23) as

$$A(x)=\left\{\frac{\chi(0)}{\chi(x)}\right\}^{1/2}\,. \quad \cdots\cdots\cdots\cdots\cdots\cdots(25)$$

The characteristic impedance $\alpha(x)$ which is a function of x is defined by

$$\alpha(x)=\lim_{dx\to 0}\frac{\chi(x-dx)}{\chi(x)}\fallingdotseq\frac{\chi(x)-\chi'(x)dx}{\chi(x)}\,, \quad \cdots\cdots\cdots\cdots\cdots\cdots(26)$$

where, $\chi'(x)$ means $d\chi(x)/dx$. The reflection coefficient $\beta(x)$ is given by substituting Eq. (26) into Eq. (3)

$$\beta(x)=\frac{1-\alpha(x)}{1+\alpha(x)}\fallingdotseq\frac{\chi'(x)}{2\chi(x)}dx\,. \quad \cdots\cdots\cdots\cdots(27)$$

So that, $B(x)$ is expressed by

$$B(x)=\frac{\chi'(x)}{2\chi(x)}\,. \quad \cdots\cdots\cdots\cdots\cdots\cdots\cdots(28)$$

3.3 Characteristics of the Ground Shaking and Considerations of the Accuracy of the Approximate Method

The characteristics of ground shaking are investigated by using two models of the inhomogeneous layer. In order to examine the accuracy of the approximate equations derived in **3.1**, the

models used are the same as those by Kobori *et al.*[12] who gave the exact solutions for them with their calculated results.

The dimensionless variable ξ is defined by the following expression in order to unify the expression of conditions of inhomogeneity;

$$\xi=\frac{x}{H}, \quad \cdots\cdots(29)$$

where, H is the thickness of the inhomogeneous soil layer. The notations for the displacement, the shear modulus, the density and the wave velocity of the superficial layer and base rock are shown in Fig. 6. The two models used are shown in Fig. 7 (A) and (B). The former is the model in which inhomogeneity is relatively small and the latter in which it is relatively large.

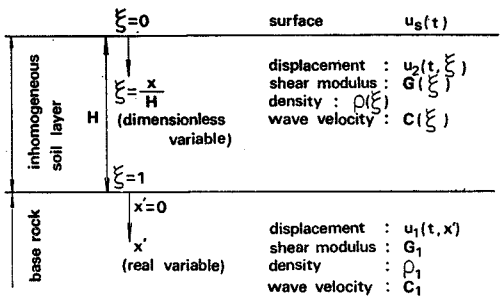

Fig. 6 Notations of Variables and Properties in an Inhomogeneous Layer.

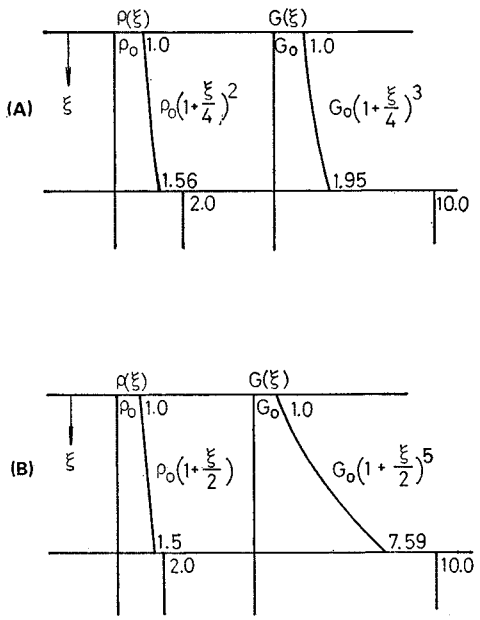

Fig. 7 The Models Used in the Analysis.[12]

Substituting Eqs. (17) and (18) into Eq. (20), the incident motion $u_0(t)$ can be expressed by the surface motion $u_s(t)$ as follows;

$$u_0(t)=\frac{A(1)}{2\gamma_n}\Big[u_s\Big(t+H\int_0^1\frac{d\xi}{c(\xi)}\Big)+\int_0^1 B(\eta)u_s\Big(t+H\int_0^1\frac{d\xi}{c(\xi)}-2H\int_0^\eta\frac{d\eta}{c(\eta)}\Big)d\eta$$
$$+\int_0^1 B(\zeta)\int_0^\zeta B(\mu)u_s\Big(t+H\int_0^1\frac{d\xi}{c(\xi)}-2H\int_\mu^\zeta\frac{d\mu}{c(\mu)}\Big)d\mu\,d\zeta+\beta_n\Big\{u_s\Big(t-H\int_0^1\frac{d\xi}{c(\xi)}\Big)$$
$$+\int_0^1 B(\eta)u_s\Big(t-H\int_0^1\frac{d\xi}{c(\xi)}+2H\int_0^\eta\frac{d\eta}{c(\eta)}\Big)d\eta+\int_0^1 B(\zeta)\int_0^\zeta B(\mu)u_s\Big(t-H\int_0^1\frac{d\xi}{c(\xi)}+2H\int_\mu^\zeta\frac{d\mu}{c(\mu)}\Big)d\mu\,d\zeta\Big\}\Big]. \quad \cdots\cdots(30)$$

Substituting the following equations into the above equation, the response of the surface in a sinusoidal steady-state for the infinite harmonic wave can be examined

$$u_0(t)=ae^{i\omega t}, \quad u_s(t)=A_se^{i\omega t}, \quad \cdots\cdots(31)$$

where, a and A_s are the amplitudes of the displacement of the incident and the surface motions respectively, i the imaginary unit and ω the angular frequency. The ratio of the amplitudes is given by the complex equation

$$\frac{A_s}{a}=\frac{2}{A(1)}\cdot\frac{1}{p+i\alpha_n q}, \quad \cdots\cdots(32)$$

where,

$$p=\cos\Big(a_0\int_0^1\frac{d\xi}{f(\xi)}\Big)+\int_0^1 B(\eta)\cos\Big\{a_0\Big(\int_0^1\frac{d\xi}{f(\xi)}-2\int_0^\eta\frac{d\eta}{f(\eta)}\Big)\Big\}d\eta$$
$$+\int_0^1 B(\zeta)\int_0^\zeta B(\mu)\cos\Big\{a_0\Big(\int_0^1\frac{d\xi}{f(\xi)}-2\int_\mu^\zeta\frac{d\mu}{f(\mu)}\Big)\Big\}d\mu\,d\zeta, \quad \cdots\cdots(33)$$

$$q=\sin\Big(a_0\int_0^1\frac{d\xi}{f(\xi)}\Big)+\int_0^1 B(\eta)\sin\Big\{a_0\Big(\int_0^1\frac{d\xi}{f(\xi)}-2\int_0^\eta\frac{d\eta}{f(\eta)}\Big)\Big\}d\eta$$
$$+\int_0^1 B(\zeta)\int_0^\zeta B(\mu)\sin\Big\{a_0\Big(\int_0^1\frac{d\xi}{f(\xi)}-2\int_\mu^\zeta\frac{d\mu}{f(\mu)}\Big)\Big\}d\mu\,d\zeta, \quad \cdots\cdots(34)$$

and α_n is the impedance ratio at the interface between the inhomogeneous layer and the base rock. a_0 is the dimensionless frequency defined by

$$a_0=\frac{\omega H}{c_0} \quad \cdots\cdots(35)$$

where, c_0 is the shear wave velocity at the surface and $f(\xi)$ is the function of ξ and shows the distribution of shear wave velocity. It is defined by

$$f(\xi)=\frac{c(\xi)}{c_0}. \quad \cdots\cdots(36)$$

The amplitude characteristic of the surface is given by the following equation from Eq. (32)

$$\left|\frac{A_s}{a}\right|=\frac{2}{A(1)}\cdot\frac{1}{(p^2+\alpha_n^2q^2)^{1/2}}, \quad \cdots\cdots(37)$$

and the phase characteristic of the surface becomes

$$\varphi_s=\tan^{-1}\frac{\alpha_n q}{p}. \quad \cdots\cdots(38)$$

By the same method as in the homogeneous elastic two-layered system, the amplitude characteristic at the bottom boundary can be calculated from

$$\left|\frac{A_H}{a}\right|=A(1)\cdot|p|\cdot\left|\frac{A_s}{a}\right|, \quad \cdots\cdots(39)$$

where, A_H is the amplitude of the sinusoidal steady-state displacement at the depth H. The functional forms for density, shear modulus, shear wave velocity, $f(\xi)$, characteristic impedance, $A(\xi)$ and $B(\xi)$ used in calculation of Eqs. (33) and (34), are summarized in Table 1 for models A and B shown in Fig. 7 (A) and (B), respectively.

Table 1 The Functional Forms for the Properties of Inhomogeneous Soil Layers about the Models A and B.

	Model A	Model B
$\rho(\xi)$	$\rho_0\left(1+\frac{\xi}{4}\right)^2$	$\rho_0\left(1+\frac{\xi}{2}\right)$
$G(\xi)$	$G_0\left(1+\frac{\xi}{4}\right)^3$	$G_0\left(1+\frac{\xi}{2}\right)^5$
$c(\xi)$	$c_0\left(1+\frac{\xi}{4}\right)^{1/2}$	$c_0\left(1+\frac{\xi}{2}\right)^2$
$f(\xi)$	$\left(1+\frac{\xi}{4}\right)^{1/2}$	$\left(1+\frac{\xi}{2}\right)^2$
$\chi(\xi)$	$\rho_0c_0\left(1+\frac{\xi}{4}\right)^{2/5}$	$\rho_0c_0\left(1+\frac{\xi}{2}\right)^3$
$A(\xi)$	$\left(1+\frac{\xi}{4}\right)^{-5/4}$	$\left(1+\frac{\xi}{2}\right)^{-3/2}$
$B(\xi)$	$\frac{5}{16}\left(1+\frac{\xi}{4}\right)^{-1}$	$\frac{3}{4}\left(1+\frac{\xi}{2}\right)^{-1}$

Model A In this model, the inhomogeneity is relatively small and the difference of rigidity between the superficial layer and the base rock is relatively large. Under the inhomogeneous condition presented in Table 1, Eqs. (33) and (34) become:

$$\begin{aligned}p=&\cos(g(1)a_0)+\frac{5}{2}[\cos(16a_0+g(1)a_0)\{C_i(8\sqrt{5}\,a_0)-C_i(16a_0)\}\\&+\sin(16a_0+g(1)a_0)\{S_i(8\sqrt{5}\,a_0)-S_i(16a_0)\}]\\&+\frac{25}{8}\int_0^1\frac{1}{4+\zeta}[\cos(8\sqrt{4+\zeta}\,a_0-g(1)a_0)\{C_i(8\sqrt{4+\zeta}\,a_0)-C_i(16a_0)\}\\&+\sin(8\sqrt{4+\zeta}\,a_0-g(1)a_0)\{S_i(8\sqrt{4+\zeta}\,a_0-S_i(16a_0)\}]d\zeta, \quad \cdots\cdots(40)\end{aligned}$$

$$\begin{aligned}q=&\sin(g(1)a_0)+\frac{5}{2}[\sin(16a_0+g(1)a_0)\{C_i(8\sqrt{5}\,a_0)-C_i(16a_0)\}\\&-\cos(16a_0+g(1)a_0)\{S_i(8\sqrt{5}\,a_0)-S_i(16a_0)\}]\\&+\frac{25}{8}\int_0^1\frac{1}{4+\zeta}[\cos(8\sqrt{4+\zeta}\,a_0-g(1)a_0)\{S_i(8\sqrt{4+\zeta}\,a_0)-S_i(16a_0)\}\\&-\sin(8\sqrt{4+\zeta}\,a_0-g(1)a_0)\{C_i(8\sqrt{4+\zeta}\,a_0)-C_i(16a_0)\}]d\zeta, \quad \cdots\cdots(41)\end{aligned}$$

where, $g(1)$ is given by

$$g(1)=\int_0^1\frac{d\xi}{\left(1+\frac{\xi}{4}\right)^{1/2}}, \quad \cdots\cdots(42)$$

and $S_i(x)$ and $C_i(x)$ are the sine and cosine integrals respectively, defined by the formula

$$S_i(x)=\int_0^x\frac{\sin t}{t}dt, \qquad C_i(x)=-\int_x^\infty\frac{\cos t}{t}dt. \quad \cdots\cdots(43)$$

The numerical results of the amplitude and phase characteristics are obtained and shown in Fig. 8. Compared with the exact solution by Kobori *et al.*,[12] the approximate technique is found to have a high degree of accuracy. It is seen from Fig. 8 that the characteristics of ground shaking do not differ so much from that of the simple layered system composed of two homogeneous layers.

Model B In this model, the inhomogeneity is

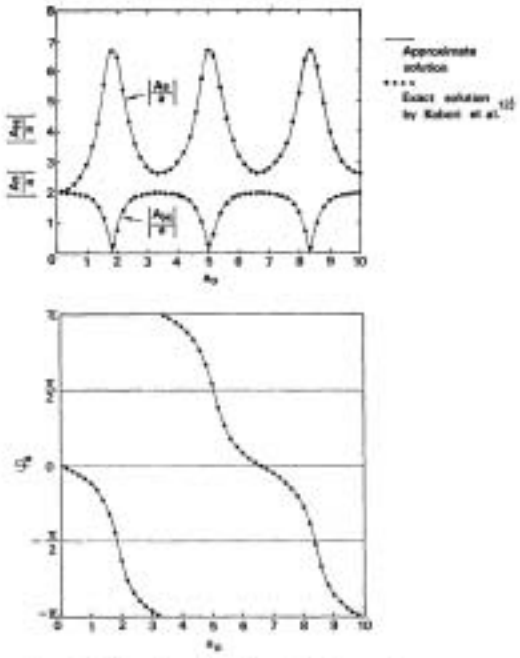

Fig. 8 The Amplitude and Phase Characteristics of Model A.

relatively large and the difference of rigidity between the superficial layer and the base rock is small. The numerical results of the characteristics of ground shaking, using the same method of calculation as described for model A, are shown in Fig. 9. Compared with the exact solution, some discrepancy appears in the low frequency range, however, it is only 3%. The tendency of the amplitude and the phase characteristics of this model are greatly different from those of the homogeneous two-layered system.

3.4 Numerical Example

The underground motions in the time domain are inferentially calculated from the observed earthquake record on the ground surface and compared with the observed one.

As the one of Abeno re-development projects, Osaka, three seismo-meters were placed at the different depth in the ground; the ground surface, 10 m and 30 m below, in the campus of Medical Science of Osaka Municipal University. Microtremors and earthquakes were observed from December, 1970 to March, 1971.[15] The one of earthquakes observed in that period is Atsumi Hanto Oki earthquake of January 5, 1971, of which magnitude is 6.3, and the maximum acceleration at the surface is 11.84 gal.

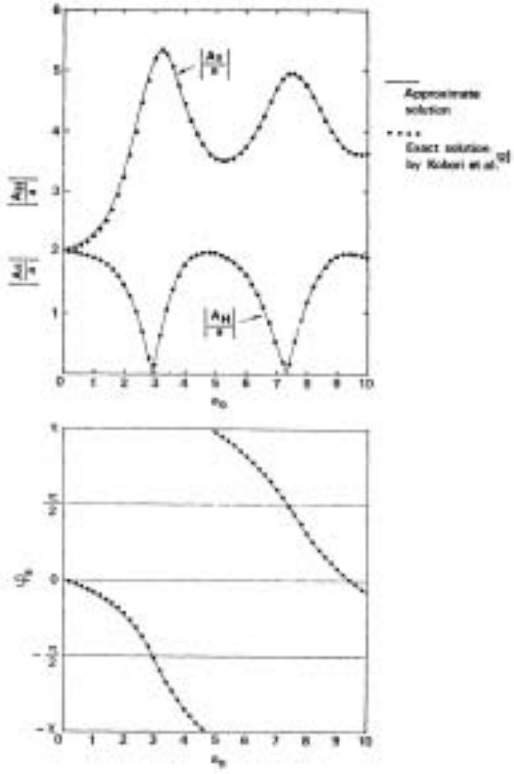

Fig. 9 The Amplitude and Phase Characteristics of Model B.

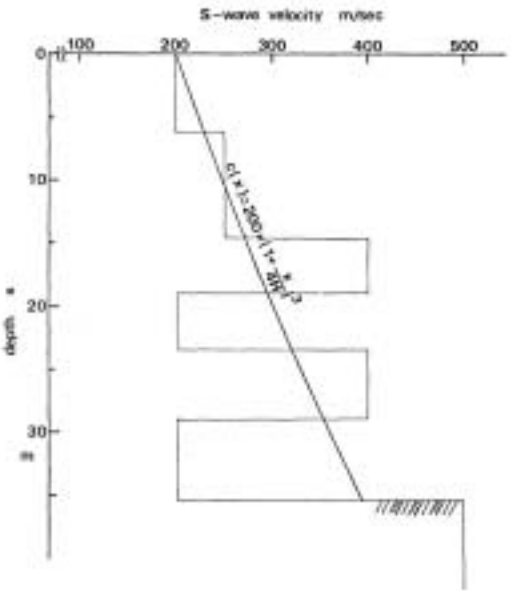

Fig. 10 Distribution of S-wave Velocity at Abeno Site.

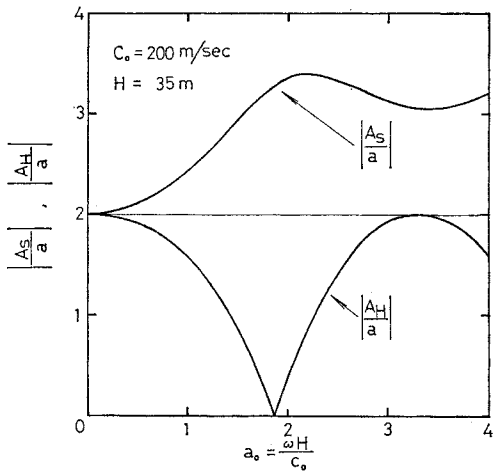

Fig. 11 Calculated Amplitude Characteristics of the Ground at Abeno Site.

A typical configuration for a distribution of S-wave velocity at the observed point is shown in Fig. 10. Though its distribution is very complicated, the distribution function of S-wave velocity is assumed as $c(x)=200(1+x/4H)^3$ for simplicity, and the layer which lies 35 m under

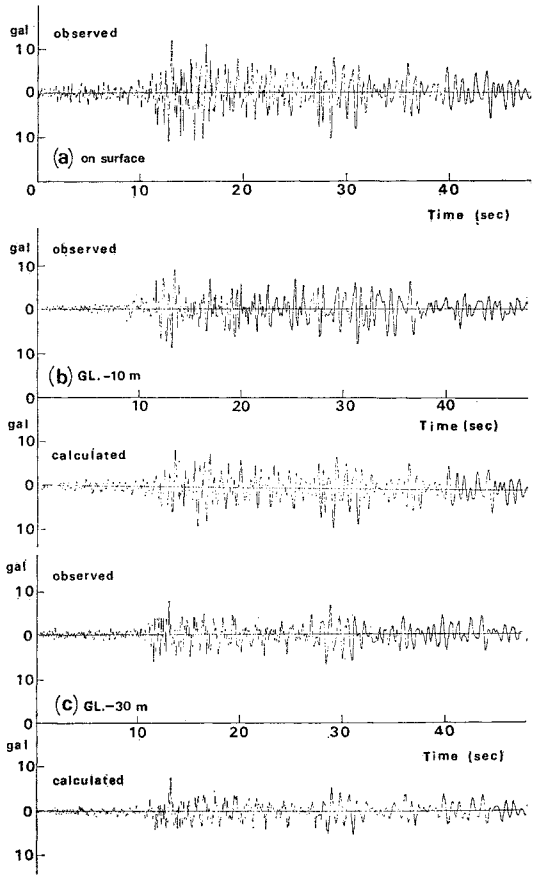

Fig. 12 The Observed and Calculated Accelerograms of Atumi Hanto Oki Earthquake. →

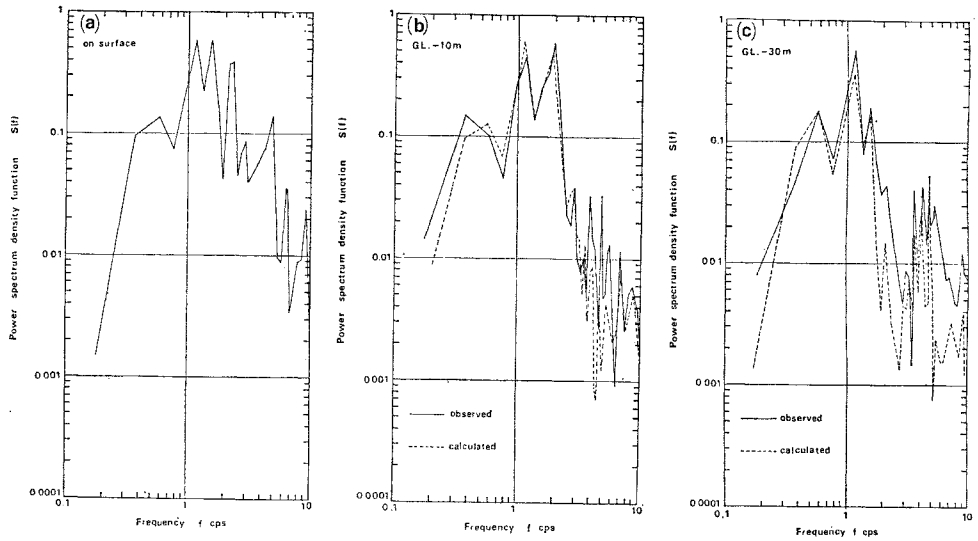

Fig. 13 Comparison of Power Spectrum Density Functions of the Observed and the Calculated Accelerograms.

the ground and in which S-wave velocity is 500 m/sec, is regarded as the base rock. The density in each layer is in the range of 1.8 to 1.9 g/cm^3 and considered to be constant through the layered soil in the analytical calculation. The amplitude characteristic of this ground is obtained by the method described in the previous section as shown in Fig. 11. It is found from this figure that the amplification at the surface is relatively small. The fundamental predominant frequency is considered to be 2 cps by using the values of $c_0=200$ m/sec and $H=35$ m.

The recorded accelerogram at the surface is shown in Fig. 12 (a). From that, the underground accelerations are computed by using Eqs. (17) to (19). The calculated accelerograms at 10 m and 30 m under the ground are compared with the observed one, as shown in Figs. 12 (b) and (c), respectively. In these figures, we can see a good agreement in the wave shapes. Figs. 13 (a), (b) and (c) show the power spectrum density functions $S(f)$ for the observed and the calculated accelerograms in Fig. 12. We notice that the component of frequency $f=1.1$ cps is prominent in all accelerograms, and that the component of frequency 2.1 cps is prominent in the surface accelerogram in spite of inferiority in the accelerogram at 30 m under the ground.

4. CALCULATION OF EARTHQUAKE RESPONSE MOTION[16]

4.1 Calculating Method

In order to calculate the surface motion as the response for the incident motion $u_0(t)$, we must calculate $u_{s1}(t)$, $u_{s2}(t)$, $\cdots$, *etc.* as indicated in Fig. 14. Then, the final surface motion $u_s(t)$ is given by

$$u_s(t)=u_{s1}(t)+u_{s2}(t)+u_{s3}(t)+\cdots . \quad \cdots\cdots(44)$$

If we adopt the approximation described in the previous section, $u_2(t)$, $u_3(t)$, $\cdots$, *etc.* can be related with u_{s1}, u_{s2}, $\cdots$, *etc.*, respectively, according to Eq. (18). Now, we compute $u_{s1}(t)$, $u_{s2}(t)$, $\cdots$, *etc.* one by one from the known function $u_0(t)$.

At first, $u_1(t)$ can be related with $u_0(t)$ as

$$u_1(t)=\gamma_n u_0(t) . \quad \cdots\cdots(45)$$

Eq. (17) for the ascending wave holds between $u_1(t)$ and $u_{s1}(t)$ and the new relation is given by

$$u_1(t)=\frac{1}{2}A(H)\left\{u_{s1}\left(t+\int_0^H\frac{dx}{c(x)}\right)+\int_0^H B(y)u_{s1}\left(t+\int_0^H\frac{dx}{c(x)}-2\int_0^y\frac{dy}{c(y)}\right)dy \right.$$
$$\left.+\int_0^H B(z)\int_0^z B(w)u_{s1}\left(t+\int_0^H\frac{dx}{c(x)}-2\int_w^z\frac{dw}{c(w)}\right)dw\,dz\right\} . \quad \cdots\cdots(46)$$

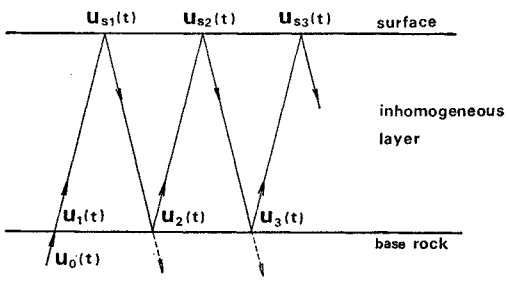

Fig. 14 Multiple Reflection of Waves.

This equation is applicable when we know $u_{s1}(t)$. However, we know only $u_1(t)$ from Eq. (45).

Then, in order to transform Eq. (46) to the equation to give $u_{s1}(t)$ in terms of $u_1(t)$, we introduce the Fourier transform. The Fourier transformation of $u_1(t)$ is given by

$$U_1(i\omega)=\frac{1}{\sqrt{2\pi}}\int_{-\infty}^{\infty}u_1(t)e^{-i\omega t}dt . \quad \cdots\cdots(47)$$

Similarly, for $u_{s1}(t)$,

$$U_{s1}(i\omega)=\frac{1}{\sqrt{2\pi}}\int_{-\infty}^{\infty}u_{s1}(t)e^{-i\omega t}dt . \quad \cdots\cdots(48)$$

By the Fourier transformation of Eq. (46), we obtain

$$U_{s1}(i\omega)=\frac{2U_1(i\omega)}{A(H)}\cdot\frac{1}{F(i\omega,H)} , \quad \cdots\cdots(49)$$

where,

$$F(i\omega,H)=\exp\left(-i\omega\int_0^H\frac{dx}{c(x)}\right)\left\{1+\int_0^H B(y)\exp\left(2i\omega\int_0^y\frac{dy}{c(y)}\right)dy\right.$$
$$\left.+\int_0^H B(z)\int_0^z B(w)\exp\left(2i\omega\int_w^z\frac{dw}{c(w)}\right)dw\,dz\right\} . \quad \cdots\cdots(50)$$

$u_2(t)$ can be obtained in terms of $u_{s1}(t)$ by

$$u_2(t)=-\frac{1}{2}A(H)\beta_n\left\{u_{s1}\left(t-\int_0^H\frac{dx}{c(x)}\right)+\int_0^H B(y)u_{s1}\left(t-\int_0^H\frac{dx}{c(x)}+2\int_0^y\frac{dy}{c(y)}\right)dy\right.$$

$$+\int_0^H B(z)\int_0^z B(w)u_{s1}\left(t-\int_0^H\frac{dx}{c(x)}+2\int_w^z\frac{dw}{c(w)}\right)dw\,dz\Big\}. \quad \cdots\cdots(51)$$

By the Fourier transformation of this equation, we obtain

$$U_2(i\omega)=-\frac{1}{2}A(H)\beta_n U_{s1}(i\omega)G(i\omega, H)\,, \quad \cdots\cdots(52)$$

where, $U_2(i\omega)$ is the Fourier transform of $u_2(t)$. $G(i\omega, H)$ is given by

$$G(i\omega, H)=\exp\left(i\omega\int_0^H\frac{dx}{c(x)}\right)\Big\{1+\int_0^H B(y)\exp\left(-2i\omega\int_0^y\frac{dy}{c(y)}\right)dy$$
$$+\int_0^H B(z)\int_0^z B(w)\exp\left(-2i\omega\int_w^z\frac{dw}{c(w)}\right)dw\,dz\Big\}. \quad \cdots\cdots(53)$$

The similar relations as Eqs. (49) and (52) hold between $U_{s2}(i\omega), U_{s3}(i\omega), \cdots$, *etc.* and $U_3(t), U_4(i\omega), \cdots$, *etc.*, respectively, as follows;

$$\left.\begin{aligned} U_{s2}(i\omega)&=\frac{2U_2(i\omega)}{A(H)}\frac{1}{F(i\omega, H)}\,,\\ U_{s3}(i\omega)&=\frac{2U_3(i\omega)}{A(H)}\frac{1}{F(i\omega, H)}\,,\\ &\cdots\cdots\cdots\cdots\end{aligned}\right\} \quad \cdots\cdots(54)$$

and

$$\left.\begin{aligned} U_3(i\omega)&=-\frac{1}{2}A(H)\beta_n U_{s2}(i\omega)G(i\omega, H)\,,\\ U_4(i\omega)&=-\frac{1}{2}A(H)\beta_n U_{s3}(i\omega)G(i\omega, H)\,,\\ &\cdots\cdots\cdots\cdots\end{aligned}\right\} \quad \cdots\cdots(55)$$

The Fourier transform of Eq. (45) is given by

$$U_1(i\omega)=\gamma_n U_0(i\omega)\,. \quad \cdots\cdots(56)$$

From Eqs. (49), (52), (54), (55) and (56),

$$\left.\begin{aligned} U_{s1}(i\omega)&=\frac{2\gamma_n}{A(H)}U_0(i\omega)\,,\\ U_{s2}(i\omega)&=-\frac{2\gamma_n}{A(H)}U_0(i\omega)\frac{\beta_n G(i\omega, H)}{\{F(i\omega, H)\}^2}\,,\\ U_{s3}(i\omega)&=\frac{2\gamma_n}{A(H)}U_0(i\omega)\frac{\{\beta_n G(i\omega, H)\}^2}{\{F(i\omega, H)\}^3}\,,\\ &\cdots\cdots\cdots\cdots\end{aligned}\right\} \quad \cdots\cdots(57)$$

Therefore, we obtain the surface motion, $U_s(i\omega)$, in the Fourier transform from Eq. (44) as follows;

$$\begin{aligned} U_s(i\omega)&=U_{s1}(i\omega)+U_{s2}(i\omega)+U_{s3}(i\omega)+\cdots\\ &=\frac{2\gamma_n}{A(H)}U_0(i\omega)\frac{1}{F(i\omega, H)}\\ &\quad\times\left[1-\frac{G(i\omega, H)}{F(i\omega, H)}\beta_n+\left\{\frac{G(i\omega, H)}{F(i\omega, H)}\beta_n\right\}^2\right.\\ &\quad\left.-\cdots\right]\\ &=\frac{2\gamma_n}{A(H)}U_0(i\omega)\frac{1}{F(i\omega, H)+\beta_n G(i\omega, H)}\,. \end{aligned} \quad \cdots\cdots(58)$$

In the above equation, $F(i\omega, H)+\beta_n G(i\omega, H)$ reduces further to

$$F(i\omega, H)+\beta_n G(i\omega, H)=\gamma_n(p'+i\alpha_n q'), \quad \cdots(59)$$

where, p' and q' are similar as p and q in Eqs. (33) and (34), respectively, and expressed as:

$$p'=\cos\left(\omega\int_0^H\frac{dx}{c(x)}\right)+\int_0^H B(y)\cos\left(\omega\int_0^H\frac{dx}{c(x)}-2\omega\int_0^y\frac{dy}{c(y)}\right)dy$$
$$+\int_0^H B(z)\int_0^z B(w)\cos\left(\omega\int_0^H\frac{dx}{c(x)}-2\omega\int_w^z\frac{dw}{c(w)}\right)dw\,dz\,, \quad \cdots\cdots(60)$$

$$q'=\sin\left(\omega\int_0^H\frac{dx}{c(x)}\right)+\int_0^H B(y)\sin\left(\omega\int_0^H\frac{dx}{c(x)}-2\omega\int_0^y\frac{dy}{c(y)}\right)dy$$
$$+\int_0^H B(z)\int_0^z B(w)\sin\left(\omega\int_0^H\frac{dx}{c(x)}-2\omega\int_w^z\frac{dw}{c(w)}\right)dw\,dz\,. \quad \cdots\cdots(61)$$

So that, Eq. (58) becomes

$$U_s(i\omega)=\frac{2}{A(H)}U_0(i\omega)\frac{1}{p'+i\alpha_n q'}\,. \quad \cdots\cdots(62)$$

When the surface motion $u_s(t)$ is known, the way to calculate the underground motion $u(t, x)$ from $u_s(t)$, has been presented in the previous section. From Eqs. (17), (18) and (19), this means that the Fourier transform of $u(t, x)$ is expressed in term of $U_s(i\omega)$ as follows;

$$U_x(i\omega)=A(x)p''U_s(i\omega) \quad \cdots\cdots(63)$$

where, $U_x(i\omega)$ is the Fourier transform of $u(t, x)$. p'' is given by

$$p''=\cos\left(\omega\int_0^x\frac{dx}{c(x)}\right)+\int_0^x B(y)\cos\left(\omega\int_0^x\frac{dx}{c(x)}-2\omega\int_0^y\frac{dy}{c(y)}\right)dy$$

$$+\int_0^x B(z)\int_0^z B(w)\cos\left(\omega\int_0^x\frac{dx}{c(x)}-2\omega\int\frac{dw}{c(w)}\right)dw\,dz\,. \quad\cdots\cdots(64)$$

Finally, we can obtain the surface motion $u_s(t)$ and the underground motion $u(t, x)$ in time domain by means of the inverse transform of $U_s(i\omega)$ and $U_x(i\omega)$, as follows;

$$\left.\begin{aligned} u_s(t)&=\frac{1}{\sqrt{2\pi}}\int_{-\infty}^{\infty}U_s(i\omega)e^{i\omega t}d\omega\,,\\ u(t,x)&=\frac{1}{\sqrt{2\pi}}\int_{-\infty}^{\infty}U_x(i\omega)e^{i\omega t}d\omega\,. \end{aligned}\right\}\quad\cdots(65)$$

In the actual computations of the Fourier transform and the inverse transform by computers, it is known to be convenient to use F.F.T..

4.2 Numerical Example

As a numerical example, the earthquake response of Osaka area will be examined by the method described in **4.1**. Osaka is a controlling city for the west part of Japan, and its population and house density have been heavily increasing. The potential of the earthquake damage becomes increasing. From a point of view of the disaster prevention, Yoshikawa and Iwasaki have throughly investigated the history of earthquakes, the response characteristics, the geological formation of Osaka area and its dynamic properties.[17),18),19)] Furthermore, they computed the ground earthquake response motions by the lumped mass method and concluded that the computed motions agreed with the recorded motions. Owing to their extensive researches, we may be able to roughly predict the behavior of Osaka ground during earthquakes.

As found later, the vertical distributions of S-wave velocity and the density through the superficial soil layer in Osaka, can be rather expressed by suitable functions. Therefore, we can easily apply this approximate technique. By this technique, the characteristics of ground shaking, response motions and the vertical distributions of maximum accelerations and shear strains during a strong earthquake are computed.

a. *Geological Formation of Osaka Area*

Yoshikawa and Iwasaki[19)] summarized the results on the dynamic properties of Osaka soils explored by many researchers, and showed the geological formations and their dynamic properties as presented in Table 2. Below the top subsurface of alluvium clay and sand layers with 0-40 m thick, 400-800 m thick diluvium layers called as Upper Pleistocene Formations, Osaka Group and Infra Osaka Group consisting of clay, sand and gravel layers and tertiary sand and clay soft rock layers called as Kobe Group and Nijo Group with thickness about 300 m, continue down to the granitic base rock which exists

Table 2 The Geological Formations of Osaka Area and Their Dynamic Properties[19)].

		Thickness (m)	S-wave velocity (m/sec)	Unit weight (g/cm³)
Alluvium	clay	0- 40	80- 190	1.5-1.6
	sand		110- 190	1.5-1.7
Upper Pleistocene Formations		400-800	200- 600	1.6-1.9
Osaka Group				
Infra Osaka Group				
Kobe Group Nijo Group		300	500- 800	2.0-2.1
Granitic base rock			2700-3000	2.7

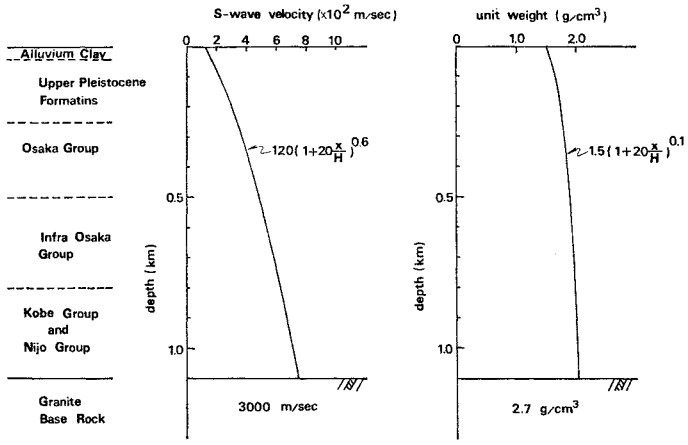

Fig. 15 The Assumed Distribution Functions of the S-wave Velocity and the Unit Weight in Osaka Ground.

about 700-1400 m below the ground surface.[20] The S-wave velocity and the unit weight of the ground are increasing nearly monotonously with the depth. For the analysis of the response, the distribution functions of the S-wave velocity and the unit weight were determined as indicated in Fig. 15, where the granitic layer was considered as the base rock. At the interface between the base rock and the bottom boundary of the surface layer, the ratio of the characteristic impedance α_n is 0.187.

b. *Incident Earthquake Motions at the Base Rock*

By the principle of the multiple reflection theory, the incident earthquake motion at the base rock was inferentially computed by using the accelerogram of El Centro earthquake of May 18, 1940. The geological formation for the El Centro location is shown in Fig. 16 which includes layer thicknesses, wave velocities and densities.[21] The layer which lies 19 m below the surface of the ground, can be considered to be the base rock. The maximum acceleration of the computed base rock motion is 76 gal (0.078 g) and the prominent period is about 0.3 sec. This is used as the base rock motion of Osaka ground in the analysis.

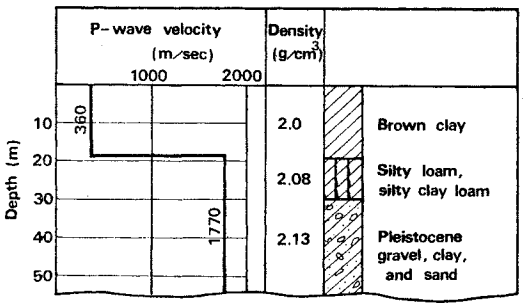

Site	First Layer				Second Layer		
	H_1	V_p	V_s	ρg	V_p	V_s	ρg
El Centro	19	360	157	2.0	1,770	843	2.08

Fig. 16 Site Characteristics at El Centro.[21]

c. *Characteristics of Ground Shaking*

The characteristic of ground shaking was calculated under the inhomogeneous conditions as indicated in Fig. 15, by the way described in **3.3.** The numerical results of the amplitude and the phase characteristics at the surface are shown in Fig. 17. It is found from the figure that the amplification of the amplitude is considerably large. The fundamental period is 8.06 sec which is a relatively long period because of taking into account the deep geological formations of 1.1 km below the surface.

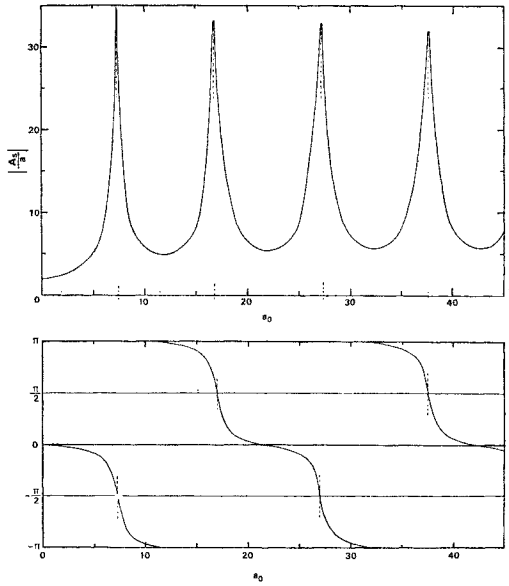

Fig. 17 Characteristics of Ground Shaking, a_0=0-45 (f=0-0.78 cps).

d. *Earthquake Response Motions on the Surface and in the Underground*

Earthquake response motions on the surface and in the underground were computed by the method described in **4.1.** The computed accelerations at the surface and 500 m below the surface are shown in Fig. 18. The maximum acceleration at the surface is 526 gal (0.54 g) and the frequency components of 0.45, 0.82 and 3.7 cps are prominent. The distribution of the maximum accelerations in the ground is shown in Fig. 19. It is found from this figure that the maximum acceleration rapidly decreases at the depth of 100 m, and 400 m below the surface, it is almost constant of about 0.15 g. That is, the earthquake motions are amplified in the top surface layer of alluvium clay and sand with relatively low rigidity.

e. *Underground Shear Strain*

From Eq. (6), the equation to calculate the the shear strain $\gamma(t, x)$ at an arbitrary depth in the inhomogeneous soil layer can be derived as follows;

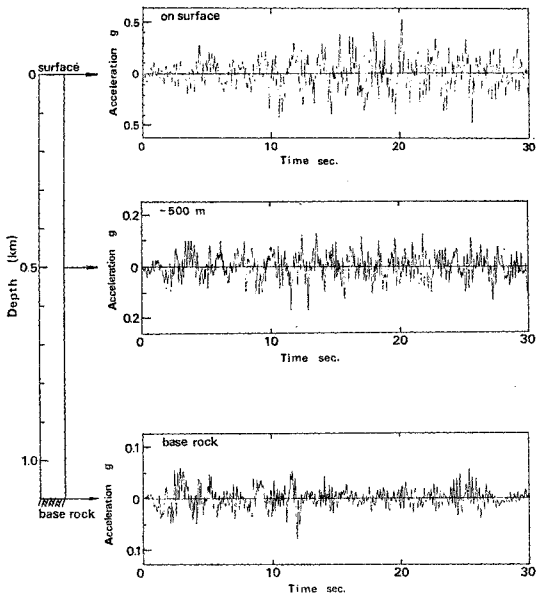

Fig. 18 Computed Accelerations at the Surface and 500 m in the Depth.

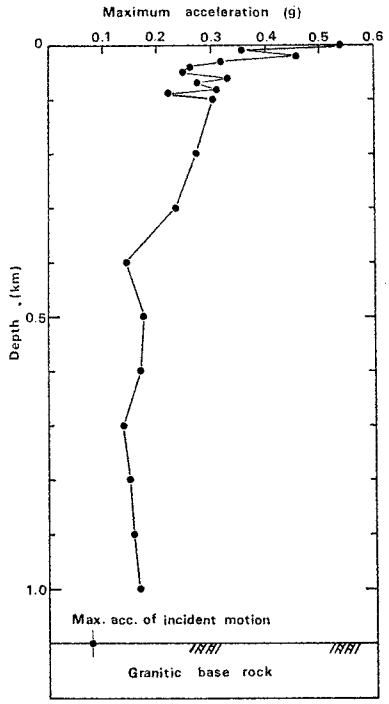

Fig. 19 Distribution of the Maximum Acceleration in the Ground.

$$\gamma(t, x)=\frac{1}{c(x)}\left\{\frac{\partial U(t, x)}{\partial t}-\frac{\partial D(t, x)}{\partial t}\right\}. \quad \cdots(66)$$

In this equation, $\partial U(t, x)/\partial t$ and $\partial D(t, x)/\partial t$ correspond to velocities of the ascending and the descending wave, respectively. By using this equation, the underground shear strain in time domain was computed, where the time variations of acceleration were integrated to obtain the time variations of velocity. The computed shear strains at the 10 m, 500 m and 1000 m in the depth are shown in Fig. 20. At near the surface, the time variation of the strain is complicated. On the other hand, as the depth increases,

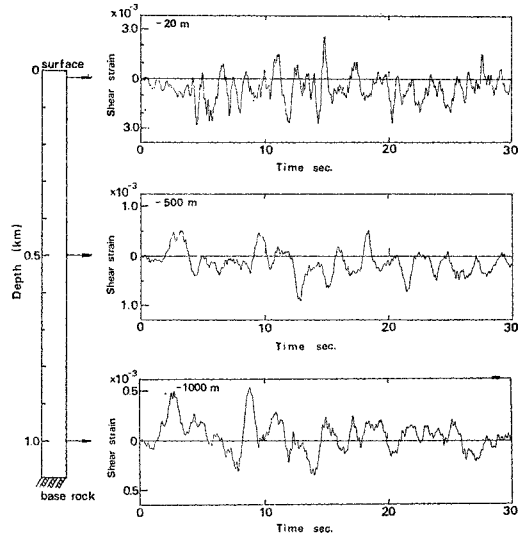

Fig. 20 Shear Strain Curves at 10 m, 500 m and 1000 m in the Depth.

the time variation of the shear strain is relatively smooth and the long period component is prominent.

From the strain curve at each depth, the maximum value of shear strain was read and plotted in Figs. 21 and 22. Fig. 21 shows the distribution of the maximum shear strain in the ground to 100 m below the surface, while Fig. 22 up to 1000 m below the surface. In the depth of 100 m, the maximum shear strain is almost constant and its value is about 3×10^{-3}, and below 100 m in the depth, the shear strain decreases and is 10^{-4} strain level below 400 m.

The computed maximum shear strains throughout the presented response analysis, are relatively large because the damping characteristics of soils are not taken into account. Below 400 m in the depth, the assumption that the soil mechanically behaves as a linear elastic material,

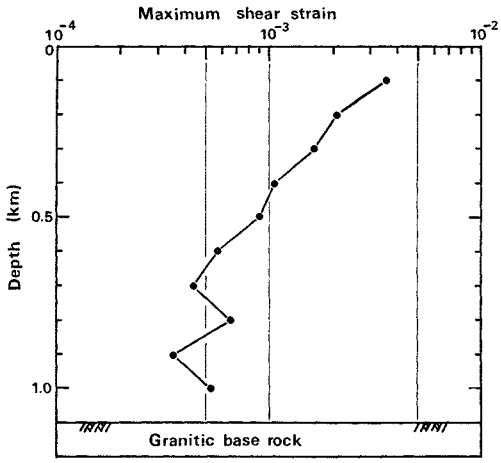

Fig. 21 Distribution of Maximum Shear Strain in the Ground Up to 100 m Below the Surface.

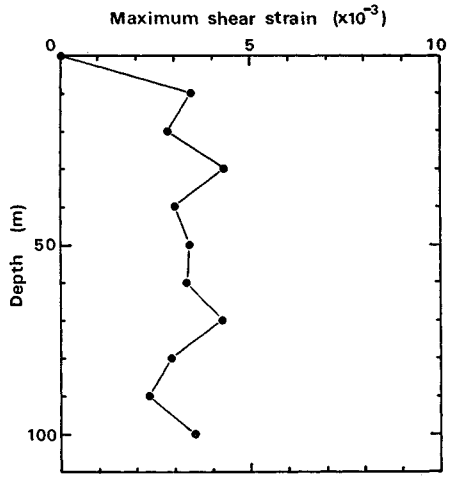

Fig. 22 Distribution of Maximum Shear Strain in the Ground.

can be accepted even for strong earthquake because of the low strain level in that depth. In the shallow depth, however, the assumption of a linear elastic body of the soil will not be valid, and it is necessary in the response analysis to take into account the inelastic behaviors of soils such as viscoelastic and elasto-plastic behaviors, and the characteristics of the strain level dependency.

5. CONCLUSIONS

When we calculate back the underground motions from an earthquake record at the surface and obtain the earthquake response of a multi-layered system, it is efficient to use the multiple reflection theory of wave for multi-layers. However, it is not often that a ground near the surface distinctly forms horizontal multi-layers, but it is rather reasonable to regard the surface layer as an inhomogeneous layer in which the vertical distribution of S-wave velocity and unit weight can be expressed by some suitable functions. In this paper, the approximate method for calculations of the underground motion and the earthquake response of an inhomogeneous ground was presented in accordance with the multiple reflection theory.

The degree of accuracy of this approximate method was examined by comparing the characteristics of ground shaking for the models of inhomogeneous ground calculated by this method with those by the exact solution. It was found that the accuracy of this method was sufficient for the engineering purposes. Moreover, the good agreement was shown between the calculated underground motions from the surface record of Atsumi Hanto Oki earthquake and ones observed under the ground during the earthquake.

The Osaka ground was considered to be an inhomogeneous layer and its earthquake response motions were obtained by applying this method. The acceleration curve at the El Centro base rock, which was calculated from the El Centro earthquake of May 18, 1940, was used as the incident motion at the granitic base rock of Osaka. Throughout the response analysis for the Osaka ground, the conclusions obtained are as follows;

(1) When we regard the granitic layer, which lies at 1.1 km below the surface, as the earthquake base rock, the fundamental period is 8.0 sec.

(2) The acceleration at the base rock is amplified about four times at the surface.

(3) According to the distribution of maximum acceleration in the ground, it decreases quickly in the depth between the surface and 100 m, and is nearly constant below 400 m.

(4) The maximum shear strain distribution is almost constant up to 100 m below the surface, and their values are about 3.0×10^{-3} strain. Below 100 m, the maximum shear strains decreases with depth and their values become about 5.0×10^{-4} strain below 600 m.

ACKNOWLEDGEMENT

The investigation in this paper was performed when the author was a doctorial course student

of Kyoto University and this was a part of the author's doctor thesis for Dr. Engineering of Kyoto University.

The author wishes to express his deepest gratitude to Professor Koichi Akai of Kyoto University, Assistant Professor Kenzo Toki of Disaster Prevention Research Institute of Kyoto University and Mr. Yoshinori Iwasaki, Chief Engineer of Osaka Soil Test Laboratory, for their providing adequate advices, stimulating discussions and continuous guidance concerned with the earthquake response analysis of grounds.

REFERENCES

1) Sezawa, K., and K. Kanai: Possibility of Free Oscillations of Strata Excited by Seismic Waves, Bull. Earthq. Res. Inst., Vol. 8, 1936, pp. 1-11, Vol. 10, 1932, pp. 1-18 and pp. 273-298.
2) Sezawa, K., and K. Kanai: Decay Constant of Seismic Vibrations of a Surface Layer, Bull. Earthq. Res. Inst., Vol. 13, 1935, pp. 251-265.
3) Kanai, K., T. Tanaka, and S. Yoshizawa: Comparative Studies of Earthquake Motions of the Ground and Underground (Multiple Reflection Problem), Bull. Earthq. Res. Inst., Vol. 37, 1959, pp. 53-87.
4) Kanai, K., T. Tanaka, S. Yoshizawa, T. Morishita, K. Osada, and T. Suzuki: Comparative Studies of Earthquake Motions on the Ground and Underground, 2nd Report, Bull. Earthq. Res. Inst., Vol. 44, 1966, pp. 609-643.
5) Toki, K.: Inference of Seismic Ground Motion from Earthquake Records, Proc. JSCE, No. 207, 1972, pp. 25-36 (in Japanese).
6) Toki, K.: Shear Stress in Surface Ground during Earthquake, Preprint, 9th Conf. JSSMFE, 1974, pp. 673-676 (in Japanese).
7) Parmelee, R. A., J. Penzien, C. F. Scheffey, H. B. Seed, and G. R. Thiers: Seismic Effects on Structures Supported on Piles Extending through Deep Sensitive Clays, Report, No. 64-2, Inst. of Eng. Res., Univ. of California, Berkeley, California, 1964.
8) Idriss, I. M., and H. B. Seed: Seismic Response of Horizontal Soil Layers, Proc. ASCE, Vol. 94, No. SM4, 1968, pp. 1003-1031.
9) Hardin, B. O., and F. E. Richart: Elastic Wave Velocities in Granular Soils, Proc. ASCE, Vol. 89, No. SM1, 1963, pp. 33-65.
10) Bhattacharya, S. M.: Exact Solutions of SH-wave Equation for Inhomogeneous Media, Bull. Seis. Soc. Am., Vol. 60, No. 5, 1970, pp. 1847-1859.
11) Upadhyay, S. K., and J. G. Negi: Effects of Varying Anisotropy Coefficient on SH-wave Dispersion, Bull. Seis. Soc. Am., Vol. 60, No. 5, 1970, pp. 2071-2081.
12) Kobori, T., R. Minai, and T. Suzuki: Wave Transfer Functions of Inhomogeneous Linear Viscoelastic Multi-Layered Media, Annuals of the Disaster Prevention Res. Inst., Kyoto Univ., No. 13A, 1970, pp. 213-232 (in Japanese).
13) Kanai, K.: Earthquake Engineering, Kyoritsu Shuppan, Co., Ltd., 1970, pp. 72-73 (in Japanese).
14) Hori, M.: On Approximate Solutions on Characteristics of Inhomogeneous Ground Shaking, Preprint, 8th Conf. JSSMFE, 1973, pp. 629-632 (in Japanese).
15) Toriumi, I.: Report on Ground Suveying in Abeno Re-Development District, 1971.
16) Hori, M.: On Approximate Solutions on Characteristics of Inhomogeneous Ground Shaking (2nd Report: on the Osaka Ground), Preprint, 9th Conf. JSSMFE, 1974, pp. 669-672 (in Japanese).
17) Iwasaki, Y.: On the Earthquake Base Rock in Osaka, Preprint, 8th Conf. JSSMFE, 1973, pp. 637-640 (in Japanese).
18) Yoshikawa, S., and Y. Iwasaki: On the Earthquake Response Characteristics and the Distribution of the Intensity of Alluvial Layer, Preprint, 26th Conf. JSCE, 1971, pp. 121-124 (in Japanese).
19) Yoshikawa, S., and Y. Iwasaki: On the Characteristics of Ground Shaking in Osaka with Considering the Deep Geophysical Formations, Preprint, 27th Conf. JSCE, 1972, pp. 221-224 (in Japanese).
20) Kobori, T., S. Yoshikawa, R. Minai, T. Suzuki, and Y. T. Iwasaki: Effects of Soil and Geological Conditions on Structural Responses in Osaka Area, Proc. Int. Conf. on Microzonation for Safer Construction Research and Application, Vol. 2, Seattle, 1972, pp. 719-734.
21) Toki, K., and S. Cherry: Inference of Subsurface Acceleration and Strain from Accelerograms Recorded at Ground Surface, Preprint.

(*Received July 15, 1974*)

コンクリートライブラリー一覧

No.	編著者	題目	定価	〒
3	委員会編	異形鉄筋を用いた鉄筋コンクリート構造物の設計例	1000	210
10	委員会編	構造用軽量骨材シンポジウム	500	140
11	樋口芳朗	微細な空げきてん充のためのセメント注入における混和材料に関する研究	120	60
15	委員会編	ディビダーク工法設計施工指針（案）改版	900	210
17	委員会編	MDC 工法設計施工指針（案）	700	210
20	委員会編	フライアッシュを混和したコンクリートの中性化と鉄筋の発錆に関する長期研究	500	100
21	委員会編	バウル・レオンハルト工法設計施工指針（案）	700	210
22	委員会編	レオバ工法設計施工指針（案）	700	140
23	委員会編	BBRV 工法設計施工指針（案）	900	210
24	委員会編	第2回構造用軽量骨材シンポジウム	1100	210
25	丸安・小林 阪本	高炉セメントコンクリートの研究	550	210
26	松本嘉司	鉄道橋としての鉄筋コンクリート斜角げたの設計に関する研究	200	80
27	岡村甫	高張力異形鉄筋の使用に関する基礎的研究	200	60
28	尾坂芳夫	コンクリートの品質管理に関する基礎研究	200	60
29	委員会編	フレシネー工法設計施工指針（案）		
30	委員会編	フープコーン工法設計施工指針（案）	1000	210
31	委員会編	OSPA 工法設計施工指針（案）	1100	210
32	委員会編	OBC 工法設計施工指針（案）	1100	210
33	委員会編	VSL 工法設計施工指針（案）	1000	210
34	委員会編	鉄筋コンクリート終局強度理論の参考	1600	210
35	委員会編	アルミナセメントコンクリートに関するシンポジウム	1300	210
36	委員会編	SEEE 工法設計施工指針（案）	1300	210

37	委員会編	コンクリート標準示方書（昭和49年度版）改訂資料	1500	210
38	委員会編	コンクリートの品質管理試験方法	1500	210
39	委員会編	膨張性セメント混和材を用いたコンクリートに関するシンポジウム	2000	210

昭和十二年二十日印刷（毎月一回）
発行（二十日発行）

野外はもちろん水中でも使用できる!!

KFW

防水型ゲージ

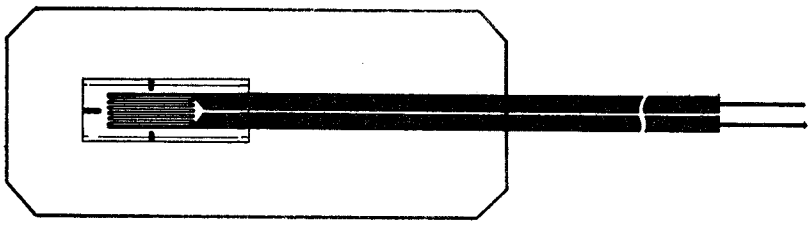

高性能な箔フェステルゲージを樹脂で覆い耐水性を高めたものです。
防湿処理が不要で、瞬間接着剤で貼るだけで野外はもちろん水中でも使用できます。
リード線も1mついています。
ゲージを楽に、短時間で接着できる現場向としておすすめいたします。

特　長

- ●野外でも防湿処理は不必要である
- ●リード線付なので、そのまま測定器へ接続できる
- ●5Rまでの曲面に使用できる
- ●水中でも使用できる（100kg/cm²で200時間）
- ●セルコンゲージである

種　類

KFW—5—C1—11	（単軸、5mm）
KFW—5—D16—11	（2軸交差、5mm）
KFW—5—D17—11	（3軸交差、5mm）

接着剤

シアノアクリレート系	CC—15A
ポリエステル系	PC—12
エポキシ系	EP—18

●**カタログお送りします**　本社開発課まで製品名、誌名記入下さい

●共和　特殊ゲージ

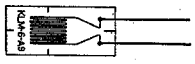

■**超大ひずみゲージ　KLM型**
約20%ひずみまで測定できる

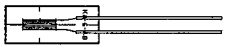

■**高温ゲージ　KA型**
300℃まで使用できる。普通鋼材ステンレス鋼材用セルコンゲージである

■**高温ゲージ　KH型**
500℃まで使用できる。接着、溶接どちらでも取付られる。

■**埋込型ゲージ　KM型**
モルタル、コンクリートの内部.ひずみを測定する

未来をひらく電子計測器メーカー
共和電業　本社・工場　〒182 調布市調布ヶ丘3—5—1　電話0424—87—2111
営業所 ——東京(502)3551／大阪(942)2661／名古屋(782)2521／福岡(411)6744／広島(21)9536／札幌(261)7629／水戸(25)1074

土木学会誌　第232号